UNITED STATES DISTRICT COURT

WESTERN DISTRICT OF NEW YORK

CAROL S. MARCELLIN, individually, and as Co-Administrator of the Estate of Charles E. Hollowell, deceased, and JESSICA HOLLOWELL-McKAY, as Co-Administrator of the Estate of Charles E. Hollowell, deceased,

Plaintiffs,

v.

HP, INC., and STAPLES, INC.,

Defendants.

Civ. No. 1:21-cv-00704-JLS

I, Quinn C. Horn, Ph.D., a competent major, depose and state as follows.

1. The statements contained herein are based on my personal knowledge.

2. I hold BS and MS degrees in metallurgical engineering and a Ph.D. in metallurgical and materials engineering. After earning my Ph.D. in 1998, I was hired by Eveready/Energizer Battery Company to lead their internal failure analysis group. Since 2004, I have been employed by Exponent Failure Analysis Associates as a technical consultant where my work has primarily focused on evaluation of safety, performance and reliability of battery systems.

3. I was retained by HP Inc., to offer an opinion regarding the alleged involvement of an HP notebook computer owned by Carol Marcellin (the "HP notebook") and, specifically, the replacement battery pack and cells therein, in a fire that occurred at 192 Bells Brook Road, Ceres, NY. on January 24, 2020.

4. My opinions are set forth in my report dated December 2, 2024.

5. As part of my work in this case, I have reviewed the reports of Steve Martin Ph.D. dated October 14, 2024 and January 3, 2025 as well as his deposition transcript in this case.

6. In support of his opinions in this case, Mr. Martin offers the opinion that there would need to be "a thermal layer temperature in excess of 300°C (572°F) for a period of over an hour for [an] external fire source to have provoked the thermal runaway reaction" in the HP notebook. In support of this opinion, Martin relies exclusively on one publication entitled: "Gas explosions and thermal runaways during external heating abuse of commercial lithium-ion graphite-LiCoO2 cells at different levels of aging." See, Larsson, F., Bertilsson, S., Furlani, M., Albinsson, I., & Mellander, B. E. (2018). *Gas explosions and thermal runaways during external heating abuse of commercial lithium-ion graphite-LiCoO2 cells at different levels of ageing*. Journal of Power Sources, 373, 220-231 attached hereto as Exhibit 1 (hereinafter the "Larsson Study").

7. I agree that the Larsson Study represents a generally-accepted academic study that can be relied upon in the field of lithium-ion batteries. However, Mr. Martin's interpretation of the Larsson Study is wrong.

8. Contrary to Mr. Martin's assertions, the Larsson Study found that all tested live cells underwent thermal runaway when externally heated to approximately 190 °C (374 °F). Thus, Mr. Martin's opinion regarding the temperature at which external heat induces thermal runaway in lithium-ion batteries is off by approximately 110 °C (230 °F).

9. The error in Mr. Martin's opinion regarding the external temperature at which thermal runway is induced in lithium-ion batteries (the "Thermal Runaway Temperature") is shown by reference to Table 4 in the Larsson Study which clearly shows that every live cell tested went into thermal runaway at an external temperature between 187 °C (369 °F) – 195 °C (383 °F) not 300 °C (572 °F):

Table 4
Temperature results from the external heating abuse tests, where ΔT is the difference b
corresponding time difference for ΔT.

Test No.	Cycle ageing and cell status	Thermal runaway temperature (°C)
1	0	195
2	0	195
3	0	192
4	0	192
5	100	190
6	100	191
7	100	187
8	200	189
9	200	188
10	300	191
11	300	> 188[a]
12	Dead cell. sudden death after 229 cycles	205
13	Dead cell. 0 cycles. stored in 60 °C during 10 months	201[b]
14	Dead cell. 0 cycles. stored in 60 °C during 10 months	203

10. Mr. Martin's error is significant to this case because he used his *erroneous* Thermal Runaway Temperature of 300 °C (572 °F) to opine that the replacement batteries in the HP Notebook caused the fire as opposed to being a victim of the fire since the temperature in the room never got to that extremely high temperature at the HP Notebook. In Martin's view, since the batteries were never exposed to external temperatures sufficient to cause thermal runaway, the only explanation for their thermal runaway had to be an internal fault i.e., they caused the fire. However, since this opinion misapplies the data in the Larsson Study, Mr. Martin's opinion that the batteries caused the fire is not reliable and is not scientifically valid.

11. On the other hand, there is evidence that that the temperature at the HP Notebook reached the *actual* Thermal Runaway Temperature in the Larsson Study [i.e., approximately 190 °C (374 °F)] because portions of the HP Notebook that were made of ABS (acrylonitrile butadiene styrene) plastic melted. The ABS so-called "process temperature" (where it can flow into molds as if melted) is in the range of 230 °C to 270 °C. Thus, exposure of the battery pack to this temperature would exceed the *real* Thermal Runaway Temperatures demonstrated by the Larsson article.

12. In other words, application of the correct data from the Larsson Study is consistent with the batteries being the victim of the fire due to exposure to external temperatures in excess of approximately 190 °C (374 °F) and not the cause of the fire.

13. Signed under the pains and penalties of perjury this 12th day of May, 2025.

Quinn C. Horn, Ph.D.

EXHIBIT 1

Journal of Power Sources 373 (2018) 220–231

Contents lists available at ScienceDirect

Journal of Power Sources

journal homepage: www.elsevier.com/locate/jpowsour

Gas explosions and thermal runaways during external heating abuse of commercial lithium-ion graphite-$LiCoO_2$ cells at different levels of ageing

Fredrik Larsson[a,b,*], Simon Bertilsson[a], Maurizio Furlani[c], Ingvar Albinsson[c], Bengt-Erik Mellander[a]

[a] Department of Physics, Chalmers University of Technology, Kemivägen 9, SE 41296 Göteborg, Sweden
[b] Division of Safety and Transport, RISE Research Institutes of Sweden, Brinellgatan 4, SE 50115 Borås, Sweden
[c] Department of Physics, University of Gothenburg, Fysikgården 1, SE 41296 Göteborg, Sweden

HIGHLIGHTS

- Gas explosions due to delayed ignition of battery emitted gases in air mixture.
- Three separate vents were detected, two vents before thermal runaway.
- Gas emissions of HF and POF_3 detected in 3rd vent with and without fire.
- Dead cells significantly less thermally reactive than working cells.
- Dead cells still undergo thermal runaway.

ARTICLE INFO

Keywords:
Gas explosion
Lithium-ion
Safety
Gas emission
Ageing
Thermal runaway

ABSTRACT

Commercial 6.8 Ah lithium-ion cells with different ageing/status have been abused by external heating in an oven. Prior to the abuse test, selected cells were aged either by C/2 cycling up to 300 cycles or stored at 60 °C. Gas emissions were measured by FTIR and three separate vents were identified, two well before the thermal runaway while the third occurred simultaneously with the thermal runaway releasing heavy smoke and gas. Emissions of toxic carbon monoxide (CO), hydrogen fluoride (HF) and phosphorous oxyfluoride (POF_3) were detected in the third vent, regardless if there was a fire or not. All abused cells went into thermal runaway and emitted smoke and gas, the working cells also released flames as well as sparks. The dead cells were however less reactive but still underwent thermal runaway. For about half of the working cells, for all levels of cycle ageing, ignition of the accumulated battery released gases occurred about 15 s after the thermal runaway resulting in a gas explosion. The thermal runaway temperature, about 190 °C, varied somewhat for the different cell ageing/status where a weak local minimum was found for cells cycled between 100 and 200 times.

1. Introduction

Lithium-ion batteries have revolutionized many products since they have a high energy density combined with several other attractive properties. Li-ion cells are used in very high numbers in e.g. cell phones, laptop computers and power tools. Besides, they are being rapidly introduced in large systems and are found in kWh to MWh energy capacity applications used in e.g. electrified vehicles, ships and stationary grid storage plants.

The use of Li-ion batteries is, however, associated with more pronounced/different risks of developed heat, gas emissions, explosions and fire compared to other battery types. These risks are yet far from being fully understood and there is a potential for increased safety through research studies as well as from the analysis of incidents. The type and the severity of the risks depend on different applications and battery system sizes. Failure consequences can be significantly increased with increasing battery system size due to cell and module failure propagation [1–3].

The Li-ion cell contains all three parts of the fire triangle that are necessary to have a fire; heat/igniter, combustible material and oxygen. Furthermore, upon overtemperatures, starting from typically 70–120 °C, the Li-ion battery starts to swell and can release gases (venting). The vented gases are flammable and toxic [4]. If the temperature is high enough, of the order of 150–200 °C, an accelerated

* Corresponding author. Department of Physics, Chalmers University of Technology, SE-412 96 Göteborg, Sweden.
E mail addresses: vegan@chalmers.se, fredrik.larsson@ri.se (F. Larsson).

https://doi.org/10.1016/j.jpowsour.2017.10.085
Received 18 July 2017; Received in revised form 22 September 2017; Accepted 26 October 2017
Available online 17 November 2017
0378-7753/

self-supporting rapid temperature increase, a thermal runaway (TR), can also occur [5,6]. The term onset temperature of a thermal runaway is referring to the temperature where the exothermic reactions starts and eventually lead to thermal runaway, while the term thermal runaway temperature refers to the very rapid temperature increase of the thermal runaway. The thermal runaway is typically associated with a release of large quantities of smoke and gas, a possible cell case rupture/explosion, fire or a gas explosion. There are thus two main types of explosions, an internal cell case explosion and a gas explosion of the flammable vented gases mixed with air. Cylindrical and hard prismatic cells can build high internal pressures and are therefore designed to release the gases via a built-in cell safety vent, however in case of e.g. a vent malfunction, extreme pressures can build up inside the battery cell, resulting in a cell case explosion. A gas explosion, on the other hand, occurs by a delayed ignition of vented combustible battery gases mixed with air accumulated in a confined or semiconfined enclosure. The consequences of a gas explosion can be significantly more severe than those of a cell case explosion.

The vented gases can contain both evaporated solvents and decomposition products, e.g. CO, CO_2, H_2, CH_4 [7–9]. Beside CO, a large number of different toxic compounds can be released [10–12] including fluoride gases. Hydrogen fluoride (HF) has caused most attention and is very toxic [13–15]. Few studies have been published that report measurements of released HF amounts from commercial Li-ion battery cells during abuse [16–20] and HF release during electrolyte fire tests [21]. The fluorine in the cells comes from the Li-salt, e.g. $LiPF_6$, but also from electrode binders, e.g. PVdF, electrode materials and coatings, e.g. fluorophosphates [22,23] and AlF_3-coated cathodes [5,24,25], as well as from fluorine containing additives, e.g. flame retardants. Battery safety is complex and a holistic perspective is essential, for example by introducing AlF_3-coatings the risk for a thermal runaway to occur can decrease while the risk for emission of toxic fluoride gases as well as for gas explosion might increase. The overall safety is therefore difficult to evaluate, it depends on battery size and scenarios, and an improvement of one parameter might actually worsen the overall safety.

There are many different types of abuse tests [26], a common one is external heating. There are several types of external heating methods for Li-ion battery cells, e.g. heating in an oven [6,26], by IR radiation [19,20,27–29], by cartridge or other heaters [30–32], in a closed chamber using e.g. accelerated rate calorimeter (ARC) [5,33] or other types [8,34,35]. So far, in most studies new/fresh cells, i.e. non-aged cells, have been tested and few studies are available investigating the influence of ageing on safety. Still it is essential to have a high battery safety level over the complete battery life time, since properties of the components may change during ageing. Ageing is typically seen in terms of calendar and cycle ageing. In order to shorten test time, storing and cycling the cells are often performed at increased temperatures, e.g. 35–55 °C, however, the results measured at these temperatures will differ from those obtained during use at ambient temperature, e.g. 20 °C, since other side and decomposition reactions may occur. The ageing processes of Li-ion cells are non-linear and complex [36–38] and not yet fully understood. For example, during ageing the solid electrolyte interphase (SEI) layer is changed and SEI plays an important role in the early stage of the thermal runaway. Abraham et al. [9] described the evolution of such modified SEI using calorimetric techniques and by quenching the temperature, described three main stages of the thermal runaway analysing the surfaces with XRD, XPS, SEM and Raman spectroscopy.

Roth and Doughty [39] studied the thermal stability of calendar aged Sony 18650 cells by ARC-tests and found that aged cells, up to 70 °C, showed higher exothermic onset temperatures. Wu et al. [40] studied 0.75 Ah non-commercial graphite/lithium cobalt oxide (LCO) Li-ion cells after 10 and 200 cycles and found that in nail penetration abuse tests the thermal safety decreased after 200 cycles. Röder et al. [41] studied 2 Ah graphite/LMO-NMC Li-ion 18650 cells stored at 60 °C up to 36 weeks and found in ARC-tests that exothermic reactions and thermal runaway onset temperatures are lower for cells aged 36 weeks. In contrast, Zhang et al. [42] studied 4.6 Ah graphite/LMO Li-ion cells stored at 55 °C for a duration between 10 and 90 days and found that the onset temperature of self-heating and thermal runaway increased for increased ageing. Fleischhammar et al. [43] studied the influence of cycle ageing on the thermal response in ARC tests for 1.5 Ah graphite/LMO-NMC high-power Li-ion 18650 cells and found significantly lower onset temperatures for first exothermic response as well as for the thermal runaway, with starting temperatures as low as 30.7 °C, and also found lithium plating on the anode for cells undergoing 1C cycling at −10 °C. Friesen et al. [44] studied safety in ARC tests of graphite/NMC 18650 fresh and cycle aged cells using 1C at 0 °C down to 70% state of health (SOH). Cells showed decreased thermal safety, aged cells had onset temperatures as low as 30 °C as well as earlier thermal runaway. The same authors also studied safety by nail penetration abuse tests and found that aged cells have a delayed but more reactive thermal runaway. In general, formation of lithium metal-plating on the anode at low temperature cycling and/or at too high charging currents poses increased risks for Li-ion batteries [43–46].

In this work Li-ion cell safety is studied for non-cycled cells stored at 20 °C and 60 °C as well as for cells aged by 100, 200 or 300 deep C/2 cycles, all cells are of the same cell type, a commercial 6.8 Ah graphite/$LiCoO_2$ Li-ion cell. The safety is assessed by abuse testing in form of external heating (oven) accompanied with FTIR gas measurements. One ARC test is performed for comparison of the safety evaluation methods.

2. Experimental

2.1. Cells tested

The cells, all from the same batch of commercially available lithium-ion cells, had nominal capacity and voltage of 6.8 Ah and 3.75 V, respectively, a LCO cathode, a graphite anode, a polymeric separator and prismatic packaging, see Table 1 for detailed cell specifications. The cells contained fluorine due to the presence of $LiPF_6$ salt in the electrolyte, however, other parts in the cell might also contain fluorine, see examples in the introduction section. Anyhow, the cell was not analyzed for other potential sources of fluorine.

2.2. Electrical characterization

Four-wire electrochemical impedance spectroscopy (EIS) in the frequency range 100 kHz - 5 mHz, with 60 points logarithmically distributed, was performed using a *Metrohm Autolab PGSTAT302N* and the *Metrohm Nova v1.11 software* in the galvanostatic mode with an

Table 1
Specification of the commercial Li-ion cell, from cell datasheet, electrolyte from TG-FTIR analysis [47] and separator from DSC-analysis [48].

Parameter	Value
Nominal voltage	3.75 V
Nominal capacity	6.8 Ah (20 °C, C/5 to 2.5 V cut-off)
Packaging	Jellyroll in aluminum hard prismatic can
Weight	140.2 g
Cycle life according to datasheet	> 70% capacity after 600 cycles with C/2 and 100% depth of discharge (DOD) at 20 °C
Max continuous discharge current	14 A
Max recommended continuous charge current	7 A
Anode	Graphite
Cathode	Lithium cobalt oxide, $LiCoO_2$
Electrolyte	Salt: lithium hexafluorophosphate, $LiPF_6$ Organic solvents: EC, DMC, EA Additives found: VC, presumable low molecular weight ketone
Separator	Shutdown separator, PE-PP

amplitude of 0.1 A. The cell was at ambient temperature, about 20 °C, in a Faraday cage. Sense and current measurement cables were twisted and separated, in opposite circles, to minimize interference.

The capacity of each cell was measured using either a multichannel *Digatron battery tester* or a *Metrohm Autolab* with *Booster 20 A module*. The capacity measurements used voltage limits of 2.50 V and 4.20 V, a current of 1.4 A (about C/5) and a cut-off charge current of 0.05 A. After the first charge, three complete discharge-charge cycles were applied. Before ageing, the discharge-capacity was measured in the first of the three cycles while after ageing the discharge-capacity of the third cycle was used to determine the cell capacity.

The battery cells were fully charged "First charge" (100% SOC) before the EIS measurement. The cycle numbers presented in this paper do not include the three charge-discharge cycles used to measure the cell capacity.

2.3. Ageing procedure

2.3.1. Ageing by cycling

The cells were cycled individually using a *Digatron battery tester*, with 100% depth of discharge (DOD) between 4.20 V and 2.50 V. The current of 3.4 A (C/2), was applied for both charge and discharge and a cut-off charge current of 0.34 A (C/20). The cells were cycled at ambient temperature, average temperature of 21 °C, with forced convection cooling. Each cell had a temperature sensor attached on the largest side surface.

2.3.2. Ageing by temperature

Fully charged cells were stored for 10 months in a 60 °C oven, which is the maximum allowed storage temperature according to the cell manufacturer's data sheet. The cells were stored at 20 °C before and after storing at 60 °C.

2.3.3. Complete cell ageing history

Firstly, the cells were stored un-used in their shipment boxes at room temperature, about 20 °C, during 12 months. Secondly, the cells underwent their first charge and the capacity and impedance was measured for each cell. Thirdly, cells selected for cycle ageing underwent cycling up to about two months (for 300 cycles). Fourthly, the capacity and the impedance were measured and the cells were stored at room temperature. Fifthly, a few non-cycled cells were selected and stored in a 60 °C oven for 10 months.

The external heating abuse tests were performed about 2 years and 4 months after the manufacturing date. Therefore, all cells were of equally long calendar age, but during their life time, some cells had been cycled and some had been stored at 60 °C for part of their lifetime (10 of 28 months).

2.4. External heating abuse tests

2.4.1. General setup

In total 14 external heating abuse tests were performed. The battery cells were individually heated using a thermostatically controlled oven, *Binder FED 115,* with an inner volume of 115 L. The battery cell was centrally placed inside the oven and mechanically fastened with steel wire (0.8 mm diameter) on a brick, see Fig. 1. The oven was turned on 1 min after the start of the test and set to 300 °C, utilizing the maximum heating rate capability of the oven. The total test time varied due to e.g. varying ambient conditions and eventual occurrence of gas explosions.

The oven was custom-made with four 50 mm diameter access ports, sealed with silicon plugs and was equipped with an internal fan set to maximum speed in order to homogenize the internal temperature. The ventilation outlet, placed on the back of the oven, was set to be fully closed. However, it was not a perfect sealing and during the abuse tests it was partially deformed. The oven door was closed by the handle in the first test but since the door opened during the gas explosion, the door was instead fastened by duct tape in the following tests. Also, one of the silicon plugs on top of the oven was attached relatively loosely, to act as a pressure vent.

Between each test the oven was lightly cleaned/washed to minimize potential interference from e.g. particle contaminations. The glass door window (triple-glass) did not mechanically break but was heavily polluted and etched so it was replaced a few times, to have reasonable video quality.

The cell voltage and temperature were measured at 1 Hz using an *Agilent 34972A* with *Agilent 34902A reed multiplexer module.* The cell voltage was measured via a type K thermocouple cable fixed by twisting the cables in small drilled holes (0.8 mm diameter) in the electrical tab connectors. The Li-ion cell surface temperature was measured using type K thermocouples attached with glass fiber tape (*3 M, electrical tape Scotch*, 19 mm wide), measured at up to six locations, T1-T6, see Fig. 1D, where T1-T4 measure the center temperature of each side,

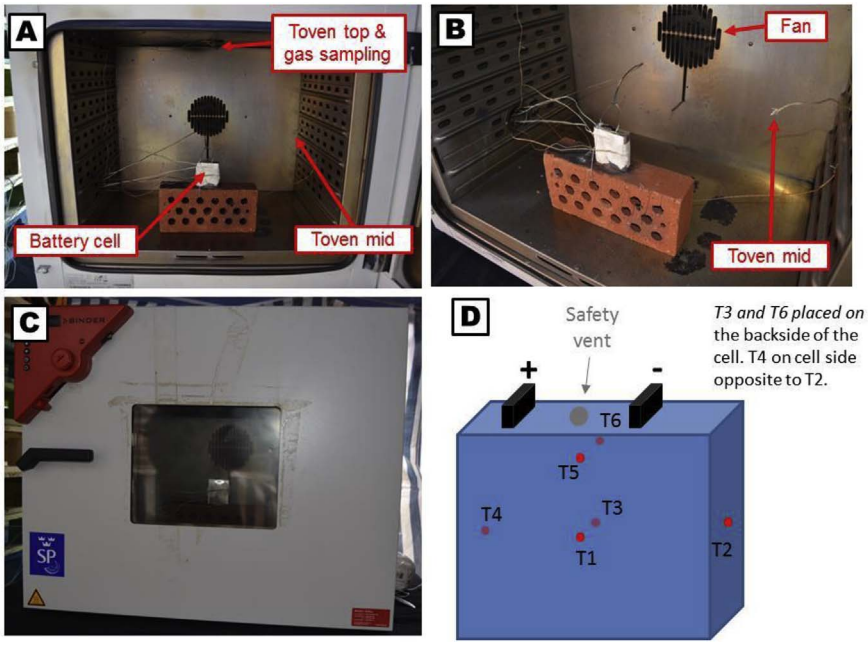

Fig. 1. Photos (**A-B**) showing the battery cell placed inside the oven, photo (**C**) showing the oven with closed door, the battery cell can be seen through the glass window of the oven door, the schematic drawing (**D**) shows the placement of the six thermocouples on the cell surface.

while T5-T6 are additional off-center sensors on the two largest surfaces. Thermocouples of type K were also used to measure the ambient temperature (outside of the oven) and the internal oven temperature, the latter one measured at two locations, as seen in e.g. Fig. 1A and B. The abuse tests were video recorded by a camera placed outside the oven door window. In some tests, a second video camera was also used, placed at a distance, varying between about 2 and 7 m, from the oven.

The cell thickness was manually measured using a caliper (gap about 150 mm long) and the cell thickness value noted was the greatest value, which was found at about the mid-mid center position on the largest side of the cell.

2.4.2. Specific setup for measurements of gas emissions using FTIR

In four of the tests, FTIR measurements of the gas emissions were performed using a *Bruker Alpha* FTIR spectrophotometer with an accuracy of 0.19 cm^{-1}. The *transmission* module was used with a gas cell of 7 cm long optical path and CaF_2 windows. The non-heated gas cell had a volume of 12.4 mL and was fed via a non-heated 0.73 m long HDPE hose of 1 mm inner diameter and 3 mm outer diameter, having a dead volume of 0.57 mL. The sampling was conducted from a central top position in the oven using an aspirator pump with a controlled flow. The temperature sensor at the top of the oven was located right at the gas outlet. All measurements and elaboration were managed with the accompanying software *OPUS v7.2* inclusive of the package *Reactmon* for sequencing.

In order to have rapid measurements, the following settings were selected: resolution of 4 cm^{-1}, average of 8 scans. This resulted in a new averaged spectrum about every 12 s and an acceptable signal to noise ratio. Atmospheric compensation for H_2O and CO_2 was applied. Two different flows were used in the experiments, 10 L/hour (test 3 and 10) and 100 L/hour (test 5 and 8). A new background scan was made before the start of each measurement series. The start times for the FTIR and the other measurements were synchronized. The time delay from gas release in the oven until detection by FTIR was approximately 1 spectrum (12 s).

For the FTIR measurements, the baseline of the background spectrum is shifting during the relatively long measurement series probably due to water condensation in the FTIR measurement cell. To compensate for such shifts, a baseline correction of each absorbance trace of a specific wavenumber against time was performed using the OPUS software built-in *Rubberband* correction method.

3. Results and discussion

3.1. Ageing – capacity fade and impedance

The cell in test 12, was supposed to be cycled to 300 cycles but failed during the cycling process after reaching 229 cycles and it was not possible to charge or discharge it any more. The cells in test 13 and 14 were initially fully charged and stored in 60 °C for 10 months and after this time the voltage had dropped to less than 1 V. The thickness of these cells had increased from 18.5 mm to 21.3 mm (about 15%), however the cell weights were not changed, indicating that the cells had not leaked or vented. All the other cells in this investigation had a thickness of 18.5 mm before and after the cycle ageing.

Capacity data prior to and after ageing are presented in Table 2. The SOH is the relative remaining capacity, calculated by the present C/5 discharge-capacity divided by the initial C/5 discharge-capacity. After the cycling, the cells had reached the following SOH, about 94% (100 cycles), 91% (200 cycles) and 89% (300 cycles). End of life (at least for the first battery life use) is generally defined as a SOH of about 70–80% and the cell datasheet states > 70% SOH after 600 cycles (Table 1), thus the tested cells are far from fully aged. The cells in test 1 and 4 had lower initial discharge capacity, as shown in Table 2, because they were cycled 3 times prior to the capacity measurements. However, even though the cells in test 1 and 4 were cycled 3 times (for details, see note in Table 2), they are here referred to as 0 cycle cells. Fig. S1 shows the C/2 discharge capacity degradation during cycling for the cycled cells.

Fig. 2 shows the impedance measurements for cells with different cycle ageing. The impedance plot, Fig. 2A, has the typical appearance for lithium-ion batteries, including high frequency inductance, depressed overlapping semicircles at intermediate frequencies and a low frequency spike, each corresponding to cell and connector impedance, SEI and charge transfer effects, and mass transport, respectively [49]. The average series resistance determined from the intersection with the real axis in the complex impedance plot in Fig. 2A for this cell type was originally 13.2 mΩ and increased after 300 cycles to 14.4 mΩ (a 9% increase). In Fig. 2B the results are plotted as phase angle versus the logarithm of frequency. Two peaks are found in this plot, one at frequencies just above 0.1 Hz and one at about 2 Hz. While the low frequency peak increases in size with increasing cycle ageing the second peak more or less disappears already after a few cycles. Anyhow, already after 3 cycles distinct differences are detected and the plot of

Table 2
Cell data for cycled and none-cycled cells, capacities measured as discharge capacities with 1.4 A (a C-rate of about C/5).

Test No.	Cycle ageing and cell status	Initial discharge capacity (Ah)	Capacity after ageing (Ah)[b]	Calculated capacity loss (Ah)	Calculated SOH (%)
1	0	6.50[c]	N/A	N/A	N/A
2	0	6.63[b]	N/A	N/A	N/A
3	0	6.56[b]	N/A	N/A	N/A
4	0	6.47[c]	N/A	N/A	N/A
5	100	6.72[a]	6.26	0.46	93.2
6	100	6.64[a]	6.23	0.41	93.8
7	100	6.62[a]	6.25	0.37	94.4
8	200	6.60[a]	6.04	0.56	91.5
9	200	6.73[a]	6.05	0.68	89.9
10	300	6.53[a]	5.84	0.69	89.4
11	300	6.68[a]	5.95	0.73	89.1
12	Dead cell, sudden death after 229 cycles	6.63[a]	N/A	N/A	N/A
13	Dead cell, 0 cycles, stored in 60 °C during 10 months	6.71[b]	N/A	N/A	N/A
14	Dead cell, 0 cycles, stored in 60 °C during 10 months	6.69[b]	N/A	N/A	N/A

[a] Using Digatron battery tester.
[b] Using Metrohm Autolab PGSTAT302N.
[c] Using Metrohm Autolab PGSTAT302N, lower value because the cell was prior charge-discharged three times using 3.4 A (C/2) with 0.34 A cutoff charge current. The impact of these three additional cycles in terms of cycling ageing is regarded as negligible.

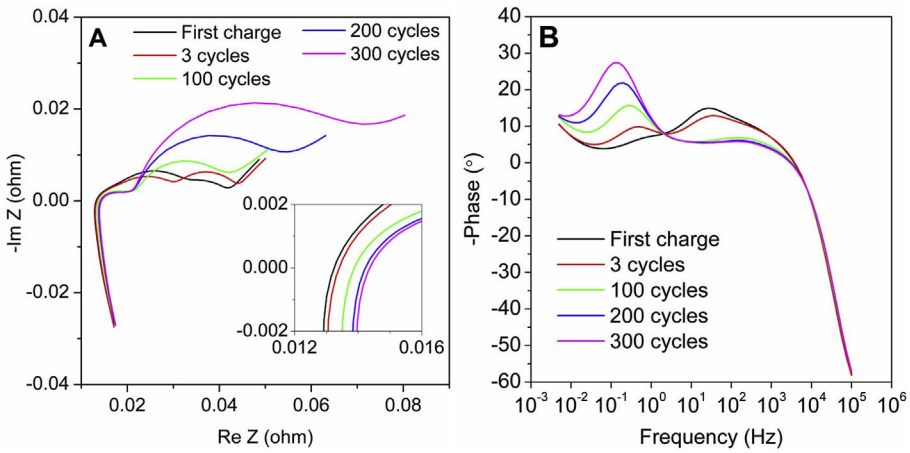

Fig. 2. (**A**) Complex impedance, between 100 kHz and 5 mHz for different number of battery cycles at 100% SOC, real vs imaginary parts with insets around the origin, and (**B**) phase vs frequency. Average values, calculated for each cycle number from all available cells, except for "3 cycles" where only one cell was measured.

phase angle thus offers another perspective to illustrate the influence of ageing. Similar plots have been published earlier for lithium-ion cells but without a more detailed discussion [50,51]. For aged batteries with same electrode chemistry (graphite/LCO) the low frequency semicircle in the impedance plot has been assigned to electrolyte oxidation at the cathode [46] and it might therefore be suggested that the growth of the peak in phase angle above 0.1 Hz in this case is also due to oxidation at the cathode. This may be likely since the cells were charged to a relatively high upper cut-off voltage of 4.20 V, yet within the cell manufacturer's specifications.

3.2. External heating abuse

In tests 1–11, the cells were fully charged (100% SOC), but had different cycling ageing, ranging from 0 to 300 cycles. The cells in test 12–14 were dead (non-functional) cells, thus the SOC was not possible to determine. The cell in test 12 suffered "sudden death" during cycling after 229 cycles. The cells used in test 13–14 had been stored for 10 months at 60 °C and had self-discharged or failed during that time and therefore had an OCV less than 1 V, that is below 0% SOC-level.

3.2.1. Overview results

Results from the external abuse tests of the fourteen cells of various ageing and status, working cells as well as dead cells, are presented in Table 3. In all tests, the temperature rate increased rapidly when the temperature reached the thermal runaway temperature, and all cells underwent a thermal runaway. For test 1–11, there were short (less than a second) and typical small flares, sparks and jet flames coming out of the cell after the thermal runaway, see examples in Fig. 3. In some cases, the cell was on fire for longer time and with larger flames, referring to the term "fire" in Table 3. The fire was typically followed by a smaller flame fire, see Table 3, which indicates the presence of one or several flames over an extended period of time. Furthermore, the terms "non-fire" or "without fire" are used when there was no ignition of the battery or its gases. This does not take into account the initial short flares/sparks/jet flames. The term "gas explosion" refers to a delayed ignition of the accumulated flammable gases released from the battery mixed with air inside the oven, which in the present case resulted in a pressure wave forcing the oven door to open. Gas explosions are common phenomena in fire science [52] however not often discussed with regard to Li-ion battery fires. In this study, as seen in Table 3, the tests for all working cells resulted either in non-fire or in a gas explosion followed by fire. Furthermore, for about half of the working cells and for all levels of cycle ageing a gas explosion occurred followed by a fire during about 30 s and a subsequent small flame fire for about 20–50 s thereafter. For the dead cells, test 12–14, the results were significantly different, the video analysis did not show any flares/sparks/jet flames, nor fire or gas explosion occurred.

For all tests, the video analysis showed that at the same time as the thermal runaway temperature was reached, the cell safety vent, located on the top of the cell, opened and released large amounts of smoke that rapidly filled up the oven volume. The color of the released smoke was typically white or light grey. In case the cell safety vent would not open, e.g. due to malfunction or bad design, a cell case explosion can occur, a dangerous situation including the risk for ejection of ballistic projectiles. This did however not occur in the present set of experiments.

The working cells lost more weight and were more swollen (thicker) than the dead cells. The weight losses were in average 22.6% for the working cells and 17.0% for the dead cells. The working cells increased their thickness from 18.5 mm to an average to 27.2 mm (an increase of 47%) while the dead cells in average were 23.8 mm thick after the external abuse. The total test times varied somewhat as seen in Table 3, resulting in different heating exposure times. Some trend was observable both on the weight loss and on the increase of thickness as function of number of cycles. These effects must have occurred within the time frame of the shortest test time (75 min, in test 6).

3.2.2. Temperature results

The temperature results from the external heating abuse tests are presented in Table 4. The thermal runaway temperature values in Table 4 are determined as the temperature when the rapid increase in temperature occurs. For working cells, the thermal runaway temperature was easily determined while for the dead cells, and in particular for test 12, it was less distinct. The dead cells have a significantly higher thermal runaway temperature, lower temperature rise rate and lower peak temperatures. The results for the dead cells with 0 cycles and stored for a part of its lifetime at 60 °C for 10 months, tests 13–14, show high reproducibility. The dead cells might still contain a large amount of flammable electrolyte, although important changes must have happened at the electrode interfaces. Cells at different SOC levels were not studied and hence any potential similarities between cells with low SOC levels and the dead cells are unknown.

The cell surface temperature sensors, T1-T6, are in general reliable at temperatures up to the thermal runaway. The thermal runaway temperature values were calculated as an average of sensors T1 and T3 for all tests except for test 13 (see note in Table 4). Above the thermal runaway temperature, the sensors record quite different temperatures and occasionally detach from the cell due to the high temperature, cell expansion and eventual gas explosions. Therefore, another average value, Tavg2, was used to find the maximum average cell surface temperature, the corresponding temperature increase (ΔT) and the time duration (step time, Δt) for that increase. Tavg2 was calculated using all usable sensors of T1-T6, specified in Table 4. Usable sensors were defined as sensors that had not lost cell surface contact. Since the number and positions of the usable cell temperature sensors varied the results presented in Table 4 naturally varies. The thermal runaway

Table 3
Overview results from external heating abuse tests.

Test No.	Cycle ageing and cell status	FTIR gas measurement	Total test time (min)	Thermal runaway and major venting[a] (min:sec)	Thermal runaway outcome Time as min:sec	Weight loss (%)	Thickness after test (mm)
1	0		105	68:39	• Flares/sparks/jet flames • No fire or explosion	22.3	25.5
2	0		127	64:24	• Flares/sparks/jet flames • No fire or explosion	22.9	26.0
3	0	YES	84	68:16	• Flares/sparks/jet flames • **Gas explosion** @ 68:30 (oven door fully opened, camera still attached and observes the accompanied fire) • 32 s fire • 14 s small flame fire (above cell vent)	22.4	27.1
4	0		84	62:55	• Flares/sparks/jet flames • **Gas explosion** @ 63:08 (oven door opened about 10 cm, camera still attached and observes the accompanied fire) • 32 s fire • 38 s small flame fire (above cell vent)	22.1	28.0
5	100	YES	84	61:54	• Flares/sparks/jet flames • No fire or explosion	23.1	27.0
6	100		75	59:22	• Flares/sparks/jet flames • **Gas explosion** @ 59:33 (oven door fully opened, camera still attached and observes the accompanied fire) • 32 s fire • 40 s small flame fire (above cell vent)	24.0	27.2
7	100		84	61:43	• Flares/sparks/jet flames • No fire or explosion	22.7	25.9
8	200	YES	94	60:39	• Flares/sparks/jet flames • Lighter **Gas explosion** @ 61:05 (door not opened, minor pressure wave on oven backside, camera still attached and observes the accompanied fire) • 81 s fire	22.2	27.8
9	200		86	62:26	• Flares/sparks/jet flames • No fire or explosion	22.8	27.2
10	300	YES	94	63:30	• Flares/sparks/jet flames • **Gas explosion @** 63:46 (oven door opened a few cm (door reclosed after about 1 min), camera blown off) • No camera to observe any fire	21.9	28.0
11	300		87[b]	61:21[c]	Power blackout[b] @ 61:17 (unfortunately just before TR) • No camera to observe any possible fire • No explosion heard, oven door not opened	22.7	29.0
12	Dead cell, sudden death after 229 cycles		84	68:36	• No flares/sparks/jet flames • No fire or explosion	14.8	23.9
13	Dead cell, 0 cycles, stored in 60 °C during 10 months		86	73:36	• No flares/sparks/jet flames • No fire or explosion	17.9	23.5
14	Dead cell, 0 cycles, stored in 60 °C during 10 months		87	72:04	• No flares/sparks/jet flames • No fire or explosion	18.2	23.9

[a] The major venting happened at the very same time as the thermal runaway temperature is reached, rapidly increasing the temperature rate. The "major venting" is also in this paper referred to as the "3rd vent".

[b] Power blackout at the test facility, data logging, oven camera and external heating switched off during about 9 min (no data logging during 9 min 39 s). Secondary video camera outside still functional (laptop-battery pack-powered) and was used to observe time for major venting and assumed to be time for TR.

[c] Determined by secondary video camera outside oven.

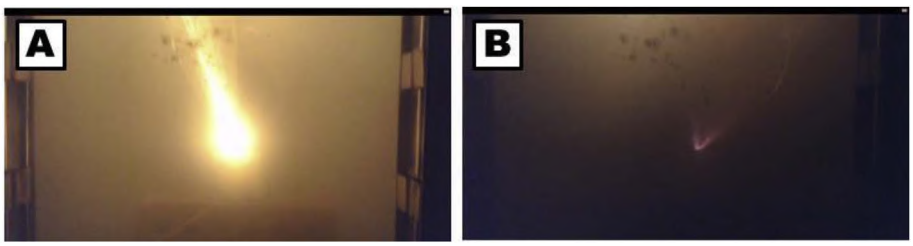

Fig. 3. Two video pictures at thermal runaway @ time 59:22 in test 6, showing a relative large jet flame **(A)** and smaller flares next after in time **(B)**, neither of them ignited the cell or the gas mixture in the oven.

Table 4
Temperature results from the external heating abuse tests, where ΔT is the difference between the Max Tavg2 and the Thermal runaway temperature. The step time, Δt, is the corresponding time difference for ΔT.

Test No.	Cycle ageing and cell status	Thermal runaway temperature (°C)	Max single sensor (°C)	Max Tavg2 (°C)	ΔT (°C)	Δt (sec)	Max dTavg2 (°C sec^{-1})	Sensors used for Tavg2
1	0	195	636	600	405	65	30	T1, T4
2	0	195	646	582	387	94	22	T1, T3, T5, T6
3	0	192	530	450	258	16	72	T1, T2, T3, T4, T5, T6
4	0	192	663	562	369	40	31	T2, T3, T5, T6
5	100	190	579	523	333	73	25	T1, T3, T4, T5
6	100	191	647	580	389	74	37	T3, T5
7	100	187	567	524	337	84	23	T1, T2, T3, T4, T5, T6
8	200	189	605	570	382	49	25	T1, T2, T3, T4, T5, T6
9	200	188	529	490	302	87	17	T1, T4, T5, T6
10	300	191	604	534	343	29	39	T1, T4, T5, T6
11	300	> 188[a]	N/A	N/A	N/A	N/A	N/A	N/A, Power blackout
12	Dead cell. sudden death after 229 cycles	205	361	339	134	129	4	T1, T2, T3, T4, T5
13	Dead cell. 0 cycles. stored in 60 °C during 10 months	201[b]	540	460	260	76	10	T3, T4, T5, T6
14	Dead cell. 0 cycles. stored in 60 °C during 10 months	203	547	463	260	75	9	T1, T2, T4, T5

[a] The average cell surface temperature was 188 °C when power blackout occurred. The thermal runaway happened about 5 s later. The average temperature curves for test 10 and test 11 followed each other very well up to the time of the power blackout.
[b] T1 thermocouple failed at the beginning of the test, so instead of calculated the average as T1 and T3, the average value was calculated using the five temperature sensors T2-T6.

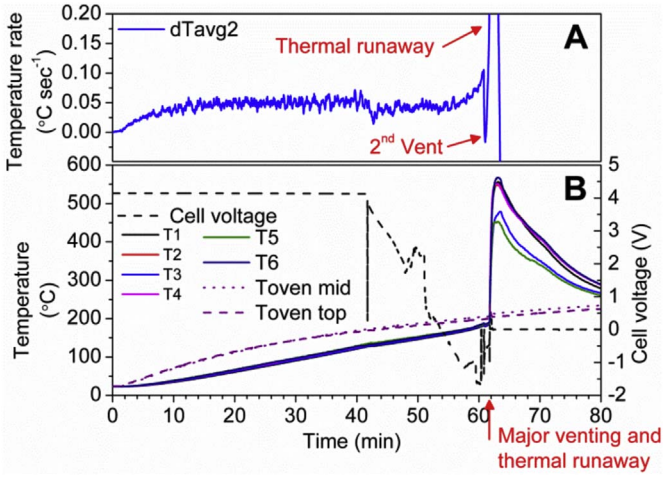

Fig. 4. Results from test 7, **(A)** showing the derivate of the average cell surface temperature, dTavg2, and **(B)** showing the cell voltage, the temperature values from the battery surface temperature sensors, T1-T6, and from the two temperature sensors in the oven, Toven mid and Toven top.

temperature values are thus rather well-defined while the maximum temperature values spread more.

The cell surface temperature sensors show relatively similar temperature values before thermal runaway, in contrast to the large temperature diversity between the sensors after the thermal runaway. Fig. 4 shows cell voltage, average temperature rate and temperature measurements for test 7, which was one of few tests having all six temperature sensors usable during the complete test. The cell surface temperatures in Fig. 4 vary up to approximately 100 °C. In other tests, local cell surface temperature variations were up to about 300 °C at the most. For this type of measurements, it is important to use multiple cell surface temperature sensors combined with proper validation methods to obtain reliable temperature measurements. The large temperature difference on the cell surface could be explained by the anisotropic heat transfer, the rapid and large heat generation, and influence from venting and fire. During thermal runaway the internal cell heat generation likely gives the highest temperature near the center of the cell. The heat transfer in the cell varies greatly in the in-plane compared to across the plane (anisotropic heat conduction) and during the heating process the thermal properties (e.g. thermal conductivity, specific heat capacity, density) of each material vary due to temperature change, due to phase change (e.g. separator melting) and due to mass loss (e.g. venting, fire) [1]. The tested cells had an aluminum case, with high thermal conductivity, yet the temperature differences are large. For other types of cell casing, e.g. pouch, even larger temperature distributions might be present.

Fig. 5A shows the average cell surface temperature prior to and during the early stage of the thermal runaway and all tests are time synchronized to the thermal runaway temperature. The temperature drops some minutes before the thermal runaway, seen for some of the curves, in particular clearly seen for the blue lines (100 cycles) and identified as due to gas release, in this paper referred to as the 2nd vent. Fig. 5B shows the thermal runaway temperature values for the working cells vs the number of ageing cycles, showing a shallow minimum between 100 and 200 cycles. The figure also shows the weight loss and the thickness after the test vs the number of cycles. In one of the tests, test 11, a total power blackout occurred at the test site seconds before the thermal runaway. The time for major venting in test 11 could anyway be determined using a battery operated outside camera. The time between the last logged data point at 188 °C and the observed gas release and its corresponding thermal runaway was about 5 s, although for a short time the temperature rate increase is relatively rapid. The temperature heating curves for test 10 and 11 followed each other very well up to the blackout.

The value of thermal runaway temperature presented in this paper is the very last temperature point before the start of the rapid temperature increase, seen in Fig. 5A. The thermal runaway temperature values presented here are about 190 °C for the working cells, and range between 201 and 205 °C for the dead cells. Similar temperature values have been reported earlier [8,26,44,53].

If the external heating had stopped at some time before the thermal runaway temperature, the cells could still go into thermal runaway depending on the cell temperature, the cells own heat-generation rate and ambient conditions such as cell cooling rate. However, the experimental method used in this work did not use a heating step increase method with pauses. Another common method used in the Li-ion battery safety field is the ARC test, according to a Heat-Wait-Search (HWS) procedure, where the battery cell is heated up with high sensitivity and the heating is halted if exothermic heat is detected from the battery cell, monitoring the exothermic cell reactions under adiabatic conditions.

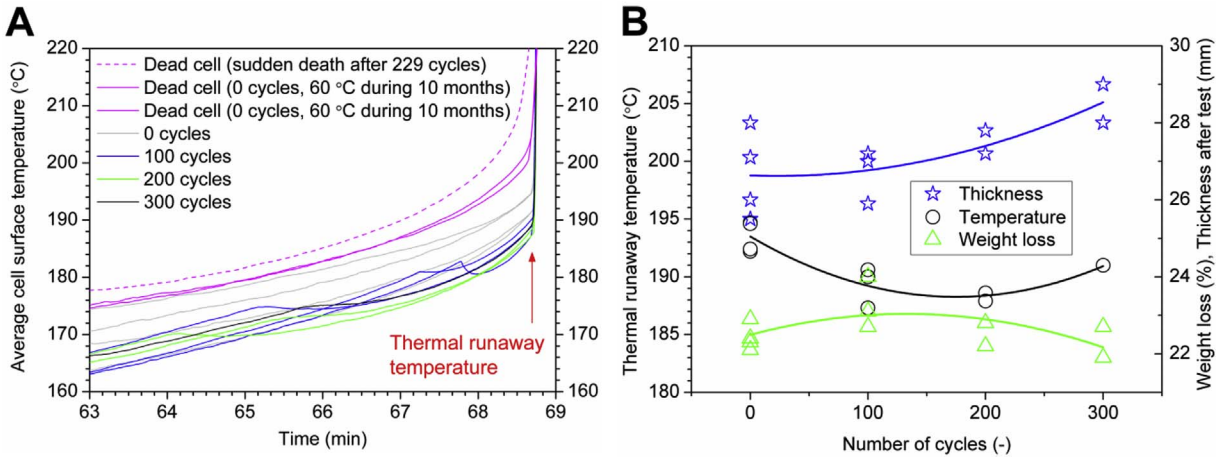

Fig. 5. The average cell surface temperature calculated as average of the sensors T1 and T3, showing **(A)** temperature vs time for all tests (the time-scales have been synchronized to the rapid temperature rise at the thermal runaway temperature, using the time in test 1 as reference time), (**B**) showing the thermal runaway temperature, cell weight loss and cell thickness after test vs number of cycles, for all working cells (the three lines are 2nd order polynominal data fit for each data type).

For ARC-measurements the onset temperature of thermal runaway can be defined as the temperature when the self-heating rate (SHR) is > 0.2 °C min^{-1} and the thermal runaway temperature when SHR > 10 °C min^{-1} [5,44]. The temperature where the exothermic reactions and the self-heating starts is test equipment specific and typically occurs when SHR > 0.02 °C min^{-1} [44].

The heating time in ARC is typically long, which allows time for boiling/venting and potential side-reactions at high temperatures to occur, e.g. electrolyte degradation and breakdown of SEI and electrode materials, which may affect the test results compared to if the cell is heated up more rapidly. In a hypothetical case, if the electrolyte would have enough time to boil/vent at lower temperatures, no thermal runaway can occur at higher temperatures since no electrolyte-electrode reactions can occur creating the thermal runaway. The heating test time of about 60 min used in the present paper, also gives time for side reactions and electrolyte boiling/venting, however less time compared to the ARC test method. As a comparison, a cell from the same batch at 100% SOC was externally abused in an ARC test by the National University of Singapore. If the thermal runaway temperature is determined from the ARC measurement in a similar way as used in the oven experiment, the result is approximately 140 °C. The temperature vs time curve can be seen in Fig. S2. The results for the two measurements thus differ by about 50 °C. The thermal runaway temperature values for the same type of cell thus depend on the test method and on its definition, as well as the location, number and measurement quality of the temperature sensor(s) used. It is crucial to be aware of this when comparing thermal runaway temperatures or onset temperature values from different studies.

The observed minimum in the thermal runaway temperature, Fig. 5B, reflects the findings of Wu et al. [40], who reported a decreased thermal stability for similar, but smaller, Li-ion cells tested at up to 200 cycles (about < 87% SOH, calculated from Ref. [40]). In that case, differential scanning calorimetry (DSC) analysis of the electrodes suggested that by ageing, part of the lithium content of the cathode is irreversibly transferred to the anode, creating a SEI layer derived by reaction with electrolyte. For 300 cycles, we observe a slightly less pronounced reactivity in terms of thermal runaway and maximum temperatures, which is only marginally associated with a diminished energy storage capability. In addition, the weight loss curve, see Fig. 5B, has a maximum corresponding to the minimum of the thermal runaway temperatures for the cells, suggesting a correlation for the two phenomena and an explanation based on the slightly higher reactivity of the cells for this stage of cycle ageing.

It is reasonable that the cell thickening, Fig. 5B, observed at the end of the test, is related to an inelastic deformation of the cell case during the thermal runaway, and in our work, it is increasing with the number of cycles. A cell thickness increase observed in dead cells before heating indicates that the irreversible deformation and thickening of the case might occur before the venting in all cases.

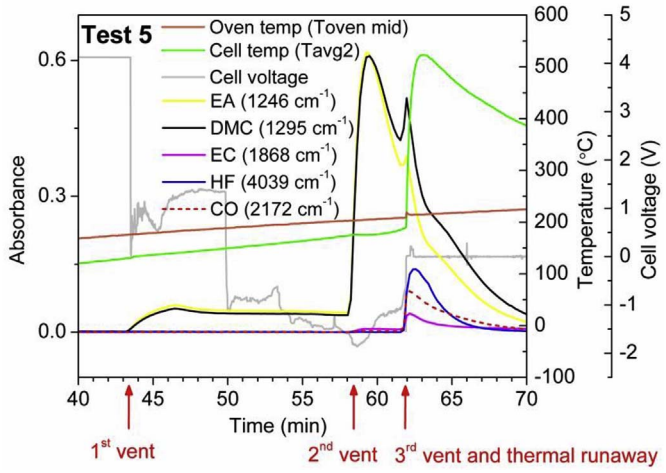

Fig. 6. Measurements of temperature, cell voltage and gas emissions for test 5 with 100 cycles. The three separate vents and thermal runaway are marked with arrows.

3.2.3. Results combined with gas measurements

Fig. 6 shows the measurements of temperature, cell voltage and gas emissions for test 5, a cell which was aged by 100 cycles. Three vents were detected. The first vent, releasing dimethyl carbonate (DMC) and ethyl acetate (EA) vapours, occurred at the same time as the cell voltage went down to about 0 V. The cell voltage drop started when the surface temperature was about 130 °C. This temperature is very close to the first melting temperature of the cell's shutdown separator, as can be seen in Fig. S3. DSC measurements on two commercial separators, one PP monolayer and one trilayer shutdown separator PP/PE/PP, as well as the separator extracted from a non-abused battery cell, are shown in Fig. S3. Due to the melting of the separator the temperature is expected to show some decrease since the process is endothermic, instead the cell surface temperature measurement clearly shows a minor temperature increase during 12 s. A possible explanation for the observed temperature increase could be that the cell undergoes an internal cell short circuit generating heat, however it should only be possible in case the shutdown separator would have a failure/melting of both separator material layers. The second vent also releases ethylene carbonate (EC),

Table 5
Flammability data for the electrolyte solvents in the cell.

Electrolyte solvent	Molecule weight (g mol^{-1})	Boiling temperature (°C) [54]	Autoignition temperature (°C) [54]	Flash point (°C) [54]	Flammable limits, lower/upper (%) [55]
Ethyl acetate (EA)	88	77	427	−3	2.2/9
Dimethyl carbonate (DMC)	90	91	458	16	4.22/12.87
Ethylene carbonate (EC)	88	248	465	143	3.6/16.1

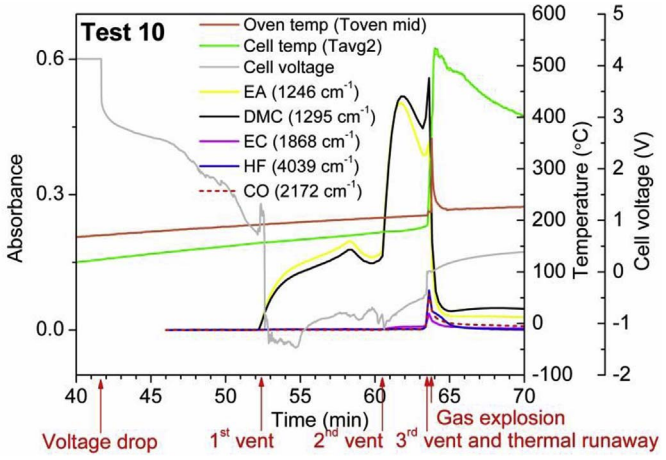

Fig. 7. Measurements of temperature, cell voltage and gas emissions for test 10 with 300 cycles. The video camera went off due to explosion so there was no camera to observe the occurrence of fire. Due to the explosion, the oven door was opened and the gas emission amounts rapidly decreased.

3.5 min before the thermal runaway, and the cell temperature clearly decreased during this venting due to the cooling effect of the outflowing gas. The first and the second vents were not seen or heard on the video, and were determined only from the FTIR gas measurement. The boiling temperature for DMC and EA is significantly lower than for EC, as seen in Table 5. The third vent, also referred to as the major venting in Table 3, occurred when the cell safety vent opened completely, the cell went into thermal runaway and the gas emissions also contained HF besides DMC, EA and EC. HF and POF_3 (not shown in Fig. 6) were simultaneously detected for the first time in the third vent/major vent that is clearly visible and audible on the video. Emission of the toxic and potentially explosive gas CO was detected in the third vent, by the appearance of its characteristic vibro-rotational bands with maxima at 2116 cm^{-1} and 2172 cm^{-1} centered around 2144 cm^{-1}. With respect to the solvent bands, the intensities of the CO bands are relatively low. Fig. 7 shows the gas emission, temperature and cell voltage results for test 10, a cell aged with 300 cycles, and the results are similar to the results in test 5, however test 10 undergoes a gas explosion. The video of the thermal runaway and gas explosion from test 10 can be seen in the supplementary materials, VideoTest10.

Supplementary video related to this article can be found at http://dx.doi.org/10.1016/j.jpowsour.2017.10.085

3.2.4. Gas explosions

For the working cells, gas explosions were relatively common, i.e. an explosion happened in 5 out of 11 cases, and happened for all levels of cycle ageing in the investigated range (0–300 cycles). In test 3, 4, 6 and 10 the oven door flung open, the camera was blown off/moved and a bang was heard when the gases in the oven ignited. For the gas explosion in test 8, the gases ignited, but the development was different, less powerful. The time between thermal runaway/major venting until ignition was 26 s in test 8 while in the other four cases the gas explosion occurred 11–16 s (with an average of 13.5 s) after the thermal runaway. If the oven had been perfectly sealed and without the pressure release counteractions, the gas explosions had probably been more severe. Videos from tests 4, 6 and 10, recorded at the time around the gas explosion, are available in the supplementary materials: in video files; VideoTest4, VideoTest6 and VideoTest10.

A comparison of temperature related data, presented in Fig. S4, shows that for cycle aged cells, the thermal runaway is somewhat delayed (occurring at a higher thermal runaway temperature) for tests having gas explosions. These tests also show higher temperature differences (higher maximum temperature), while cells with no cycle ageing (0 cycles) shows the opposite trend. Thus between 0 and 100 cycles the reversed trend is influenced by the initial ageing before 94% SOH.

For the 300 cycle cells adequate data exists unfortunately only from one test and consequently the trend above 200 cycles cannot be properly assessed. A common trend is anyhow that the maximum temperature rise rate is highest for all tests undergoing gas explosions, independent of cycle ageing, see Table 4 and Fig. S4, with maximum values ranging between 25 and 72 °C sec^{-1}. Test 1 had a maximum value of 30 °C sec^{-1}, hence the cell might have been close to a gas explosion, however, it did not happen and neither the gases nor the cell did catch fire.

A general trend regarding the occurrence of gas explosions is difficult to find from the test matrix. It is anyhow surprising that close to half of the tested cells, for all cycle ageing levels, did undergo a gas explosion, a result we consider accidental.

The cycle ageing up to 300 cycles, resulted in up to about 10% capacity drop (90% SOH) as well as a growth in impedance (series resistance) up to of about 10%. Hence, the ageing effect on safety was not fully studied. Future studies might find the occurrence of gas explosions and other thermal effects to increase, be similar or decrease by ageing. The resistance increase can be associated with SEI formation, and the thickness, morphology and composition of the SEI affects the heat generated at breakdown at a pre-stage of thermal runaway. The ageing effects of the electrolyte are not well studied however we still considered it flammable.

The formation of Li-metal (Li-plating) at the electrode(s) due to cycling is assumed to be minor, since the cycling was performed at room temperature and without extreme current rates. The influence of Li-plating, if present, on the thermal runaway is likely combined with the thermal reaction of the lithiated graphite anode with the electrolyte and dependent on the external heating abuse type.

From the video analysis, it was seen that all working cells, test 1–11, generated visible flames and sparks, however even if the oven was filled with released smoke and emitted gas no ignition occurred until at a later stage. For an explosion to occur, the mixture of gases and air must be within certain limits and an ignition source must be present. In the first about 10 s of battery gas emissions from the 3rd vent, these criteria might not have been fulfilled. The smoke and gas in the 3rd vent filled the oven in about 2–3 s and thereafter it was not possible to clearly determine the presence of flames or sparks from the video due to the low visibility in the smoke. Before the third vent/thermal runaway, the oven was filled with gas emissions originating from the 1st vent as well as the significantly larger release of the 2nd vent detected by FTIR, so the jet flames and sparks observed just after the safety vent opened in the third vent did not ignite these gases, in none of the tests.

For all cells with 0, 100 and 200 cycles the cell thickness expansion was larger if the cells had gone through a gas explosion, for the 300 cycle cells, it was the opposite. The fact that cells involved in a gas explosion were thicker might indicate that those cells did build up a higher pressure and temperature (see Fig. S4) inside the cell before the safety vent opened completely.

It is not possible to exactly determine the ignition source when the gas mixture finally ignited. The ignition could have started inside or outside the cell. The ignition source of the gas explosion could e.g. be due to non-observed sparks or flames originating from the thermal runaway, or an internal cell short circuit due to separator melting, or simply by autoignition of the hot gas mixture. The cell surface temperature was at least for some time higher than 465 °C for all working cells, thus above the auto ignition temperature for EA, DMC and EC, see Table 5. The gas explosion might potentially be due to ignition of other released battery gas products, e.g. CO and H_2. CO release was observed in all tests with gas measurements but only in the third vent. The intensities of the CO bands were relatively low compared to that of the solvents, and there was no difference in intensity for tests with and without gas explosions. Furthermore, the cell internal temperature was probably higher than the measured surface temperature. The cell might possibly contain flame retardants in the electrolyte. This might explain why none of the cells had an instant ignition and not all tests had a delayed gas ignition/gas explosion.

Table 5 shows flammability data for EA, DMC and EC. The autoignition temperature is the lowest temperature at which a flammable mixture of the solvent can spontaneously ignite. The flashpoint is the lowest temperature at which the liquid can be ignited with an ignition source. Within the flammability range, between the lower and the upper flammability limit, a gas mixture can be ignited and cause a gas explosion. When a flammable mixture is ignited it will typically expand 5–8 times due to the temperature increase, i.e. it will cause an overpressure of 5–8 bar if confined. Note that many building structures such as doors and windows can withstand a pressure difference of less than 100 mbar. A rather small amount of electrolyte is needed in order to create a flammable mixture. In one cubic meter about 30 L (3% of 1 m^3) of solvent in the gas phase is needed. Using the ideal gas law and normal temperature and pressure, one obtains that 30 L corresponds to about 100 g of solvent. This means that evaporating 1 kg of electrolyte, corresponding to about 350 Ah, solvent can result in a flammable mixture of 10 m^3.

For the 115 L volume of the oven, 100 g m^{-3} corresponds to about 12 g (8% of the cell weight) of released electrolyte that will result in reaching the lower flammability limit (LFL) in the oven. The working cells lost between 31 and 34 g in weight, while the dead cells lost 21–26 g, and the material sprayed during the vents consists of several cell parts, e.g. electrolyte, separator, etc, indicating that LFL would probably be reached relatively easy in all the tests, yet not all did ignite/explode. It is important to consider that due to the non-ideal behavior of gases and gas mixtures the LFL might vary from the one stated for each gas and also the gas concentration will have some variations within the oven volume. Besides, the rapid expansion of the gases in the oven at the increasingly high temperatures might have produced a lean oxygen environment, changing the conditions for ignition.

3.2.5. Toxic gas emissions

Gas emissions of CO, HF and POF_3 were measured in all four tests where the FTIR gas measurement was employed, regardless if there was a fire or not. CO is an asphyxiant gas. HF is very toxic while POF_3 can be seen as a precursor of HF by hydrolysis and therefore may be considered toxic. The sources of fluorine can be several as discussed in the introduction, however a major fluorine source is typically the Li-salt $LiPF_6$ producing HF and POF_3 according to Yang et al. [56],

$$LiPF_6 \rightarrow LiF + PF_5 \quad (1)$$

$$PF_5 + H_2O \rightarrow POF_3 + 2HF \quad (2)$$

$$POF_3 + 3H_2O \rightarrow H_3PO_4 + 3HF \quad (3)$$

As seen from eqs. (2) and (3), water/humidity is needed in order to produce HF. The cell interior, e.g. the electrolyte, might contain very small traces of water but they generally disappear in the first cycles of the battery by contributing to the formation of the SEI layer. In normal conditions and at moderate temperature increase, the cell is still fully sealed. When the cell sealing breaks, at the 1st vent, gas emissions are let out in oven air which contains humidity. There is thus a potential for humid air to react with cell materials in the 1st and 2nd vents, however HF and POF_3 are not yet detected. The large cell opening of the cell safety vent occurs in the third vent, and this is the only vent phase where HF as well as POF_3 are detected.

It is an interesting question why HF and POF_3 are detected only in the 3rd vent and not during the 1st and 2nd vents where the cell is open. Possibly, in the first and second vents the electrolyte solvents are boiling off and emitted as single compounds without the Li salt. In the third vent, the gas release is so strong, as is clearly observed from video, that it can release not only the most volatile part of the electrolyte but the remaining electrolyte including part of the $LiPF_6$. Thereafter the $LiPF_6$ containing electrolytes can react with the humidity in the oven and produce HF and POF_3.

The temperature also influences the HF formation, however the temperature differences in the three vents are relative low. For the four tests having gas measurement, the temperature of the gas sampled at the gas outlet, was 174–185 °C in the first vent and 193–197 °C in the second vent. In the third vent, where HF and POF_3 were detected, the temperature ranged between 203 and 240 °C and the air temperature rose to more than 300 °C in the cases when a gas explosion occurred. The gas temperature was however recorded in the oven and not in the FTIR gas cell. Anyhow, during the external heating, warm oven air is continuously sucked into the gas sampling tubes and gas cell thus warming them. For the higher flow rate used in test 5 and 8, the gas volume of the sampling system (hose and gas cell) was about 13 mL while the flow rate was about 28 mL s^{-1}, so ambient cooling effect was probably relative low. For the lower flow rate used in test 3 and 10, about 2.8 mL s^{-1}, the refilling time was anyway less than 5 s. It should also be noted that the gas sampling flow rates correspond to about one or less volume change of the oven volume, which is 115 L, per hour. The oven is not perfectly air tight so a relatively small yet essential air inflow facilitates more time-accurate FTIR measures. Conversely, when the oven door opened due to gas explosions, the FTIR gas emission data did not show accurate data.

Fig. 8A shows a FTIR vibro-rotational spectrum of HF vapor originating in the oven, and Fig. 8B shows detection of POF_3 at an earlier time in test 5. POF_3 is detected by its characteristic band at 1416 cm^{-1}, which is assigned to the prohibited Q-branch of the stretching mode [56]. The nearby bands at 1456 cm^{-1} and 1375 cm^{-1} correspond to residual evaporation of DMC [57] and EA [58], respectively. Simultaneously the P-F asymmetric stretching mode of POF_3 is also detected at 989 cm^{-1} [56]. The time sample at 79.6 min of the test 5 in Fig. 8A shows that HF is still present at 79.6 min, that is 17.7 min after the thermal runaway temperature. The FTIR measurement shows that HF is present during a longer time than POF_3 which can be explained by that POF_3 is a less chemically stable intermediate compound, decomposing according to eq. (3). These fluorinated gases could be adsorbed and/or react on the surfaces, e.g. on the oven inner walls, resulting in lower, but not less synchronized, observed gas emissions.

3.2.6. Gas detection

The gas emissions released from a Li-ion battery are both toxic and flammable. If the gas is not immediately ignited there is a risk for a

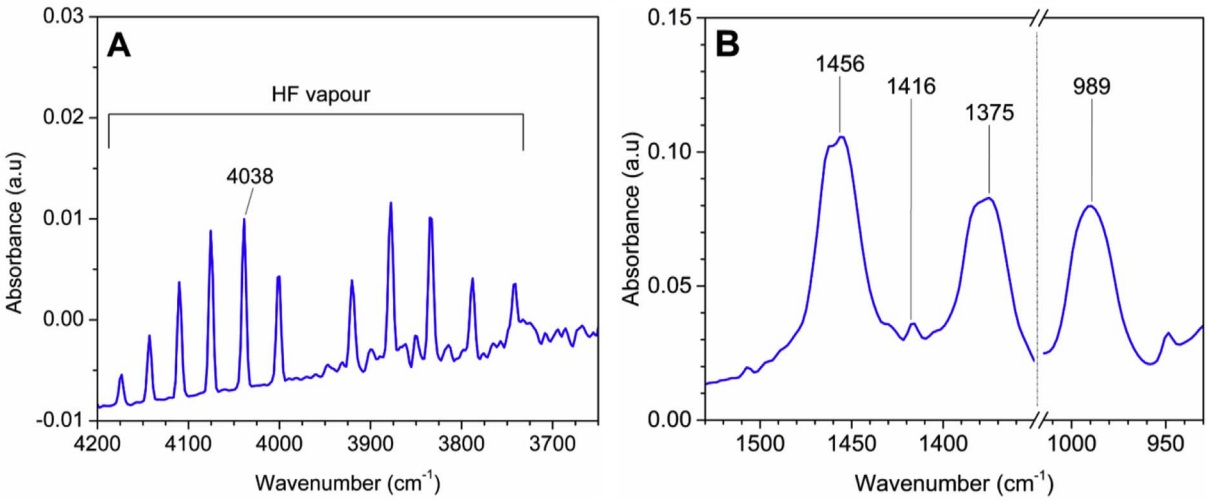

Fig. 8. FTIR measurement in test 5, (**A**) showing HF emission at time 79.6 min and (**B**) showing POF_3 emission at time 61.8 min.

delayed ignition when the flammable gas-air mixture reaches the flammability range in case there is an ignition source, e.g. the hot battery cell itself. If the gases are confined by e.g. the battery system box itself or in the outer installation box/room, this will result in a potentially severe gas explosion.

In particular for large Li-ion battery systems, it can be an essential strategy to have the ability to collect gas emissions and ventilate them out in a safe way. If gas sensors are used, they could possibly detect the level of hydrocarbons and the gas explosion risks. Gas sensors could also be used to detect toxic gases, e.g. HF sensing. There might therefore be a need of having multiple and dynamic gas sensors to detect early cell venting. The first and second vents detected in the present tests are not visually observed or audible and thus not easily detected without gas sensors. However, the cell heavily equipped with six cell surface temperature sensors, shows a temperature drop when the gases are released in the second step. The first vent is not clearly seen in the temperature data, but it indicated by the voltage drop to 0 V. A voltage drop to 0 V can indicate other types of events with and without gas release.

The second vents are quite clearly seen in Fig. 5A, when the average cell surface temperature suddenly drops, just a few minutes before the thermal runaway. The change in temperature rate in the second vent is also clearly seen in Fig. 4, where the dTavg2 rapidly drops before its very rapid increase at the thermal runaway temperature. Adequate cell surface temperature sensor(s) in a battery pack could therefore potentially predict and detect a large release of gas. Battery packs of today typically do not have one temperature sensor per cell, instead e.g. 1–2 temperature sensors per battery module (e.g. 20 cells) are used. Anyhow, there is no universal standard and this type of sensing can vary a lot, making presumed gas detection warnings from battery cell surface temperature measurements not functional, except in case of a gas release in cell(s) in direct contact with the installed temperature sensor. The major venting during cell safety vent opening that releases large amounts of smoke and gas, is rather easily seen visually. Battery systems typically have a high tightness class, e.g. IP67, which hinder gas release and visual detection and potentially increase the risks of gas explosion if gases are finally released. Without detection of vented gases, it may be impossible to eliminate a situation in which an imminent gas explosion is present, where released flammable gases are accumulated inside the battery, and only an ignition source stands between the occurrence of a gas explosion. Situations like this could be detected via gas sensors installed into the battery box. A well safety categorized battery with a strategically planned temperature detection system might also give a secondary but early measure of gas emissions.

4. Conclusions

Hard prismatic $LiCoO_2$-graphite cells with a nominal capacity of 6.8 Ah were abused by external heating in an oven. The study included cycle aged cells, non-cycled cells stored at 60 °C as well as non-cycled cells stored at room temperature. Both working and non-working (dead) cells were investigated. Upon external heating, all cells underwent thermal runaway releasing smoke and gas. For about half of the working cells, the gases accumulated in the oven ignited causing a gas explosion about 15 s after the thermal runaway and accompanied with a major smoke and gas release. Whether the cells had or had not been the subject of cycling did not influence the occurrence of the gas explosions, they occurred at all cycle ageing levels from 0 to 300 full deep cycles. The cells were aged to about 90% SOH and future studies are needed to investigate safety upon end-of-life criteria, preferably below 50% SOH in order to include second life use. Future studies are also needed to understand the mechanisms between ageing and safety. The gases were analyzed using FTIR. Gas emissions of toxic hydrogen fluoride were detected both with and without fire. Consequently, no fire was required for HF production and after a fire HF emissions were still present. The fire influence on HF production rate levels was not studied. Another emitted potentially toxic gas and a HF precursor, POF_3, was also detected simultaneously with HF. The hazardous gas CO was also detected in the 3rd vent. The thermal runaway temperature was about 190 °C and was shown to have a weak correlation with the number of cycles in the ageing process, having a minimum value between 100 and 200 cycles, within the tested cycle range of 0–300 cycles.

Three dead cells were tested, one that experienced sudden death during cycling after 229 cycles and two cells that had not been cycled but instead stored at 60 °C for 10 months. The dead cells also went into thermal runaway; however, they were significantly less reactive with increased thermal runaway temperatures and a lower rate of temperature increase. These cells did not emit any sparks or flames and there was no resulting fire or gas explosion. The work presented here shows the importance of a full assessment of the gases released, their toxicity, flammability and conditions for explosion, in order to be able to design appropriate safety measures in the application and also to be able to select what cells to use in different applications. The monitoring of the temperature and of gas release is shown as a method of an early detection of gas threat and an imminent thermal runaway.

Acknowledgements

The Swedish Energy Agency and Carl Tryggers Stiftelse för Vetenskaplig Forskning are acknowledged for their financial support.

Several persons at RISE Research Institutes of Sweden and Chalmers University of Technology have been involved in this work and are gratefully acknowledged, especially Sven Byheden for cycle ageing, Ingvar Karlson for support during abuse testing and Antti Rytinki for capacity and impedance measurements. Prof. Lu Li, National University of Singapore, is acknowledged for conducting the ARC measurement.

Appendix A. Supplementary data

Supplementary data related to this article can be found at http://dx.doi.org/10.1016/j.jpowsour.2017.10.085.

References

[1] F. Larsson, J. Andersson, P. Andersson, B.-E. Mellander, J. Electrochem. Soc. 163 (2016) A2854 A2865.
[2] C.F. Lopez, J.A. Jeevarajan, P.P. Mukherjee, J. Electrochem. Soc. 162 (9) (2015) A1905 A1915.
[3] J. Lamb, C.J. Orendorff, L.A.M. Steele, S.W. Spangler, J. Power Sources 283 (2015) 517 523.
[4] E.P. Roth, C.J. Orendorff, Electrochem. Soc. Interface summer 2012 (2012) 45 49.
[5] D. Doughty, E.P. Roth, Electrochem. Soc. Interface summer 2012 (2012) 37 44.
[6] F. Larsson, P. Andersson, B.-E. Mellander, Batteries 2 (2016) 9.
[7] J. Lamb, C.J. Orendorff, E.P. Roth, J. Langendorf, J. Electrochem. Soc. 162 (10) (2015) A2131 A2135.
[8] A.W. Golubkov, D. Fuchs, J. Wagner, H. Wiltsche, C. Stangl, G. Fauler, G. Voitic, A. Thaler, V. Hacker, RSC Adv. 4 (2014) 3633 3642.
[9] D.P. Abraham, E.P. Roth, R. Kostecki, R.,K. McCarthy, S. MacLaren, D.H. Doughty, J. Power sources 161 (2006) 648 657.
[10] J. Sun, J. Li, T. Zhou, K. Yang, S. Wei, N. Tang, N. Dang, H. Li, X. Qiu, L. Chen, Nano Energy 27 (2016) 313 319.
[11] N.P. Lebedeva, L. Boon-Brettz, J. Electrochem, Soc. 163 (6) (2016) A821 A830.
[12] A. Nedjalkov, J. Meyer, M. Köhring, A. Doering, M. Angelmahr, S. Dahle, A. Sander, A. Fischer, W. Schade, Batteries 2 (2016) 5.
[13] Documentation for Immediately Dangerous to Life or Health Concentrations (IDLHs) for Hydrogen Fluoride (As F), The National Institute for Occupational Safety and Health (NOISH), 1994.
[14] ISBN: 0-309-53013-X, Acute Exposure Guideline Levels for Selected Airborne Chemicals: Volume 4, Subcommittee on Acute Exposure Guideline Levels, Committee on Toxicology, National Research Council, 2004.
[15] A. Middelman, Hygiensiska gränsvärden AFS 2015:7, Hygieniska gränsvärden. Arbetsmiljöverkets föreskrifter om hygieniska gränsvärden och allmänna råd om tillämpningen av föreskrifterna, ISBN 978-91-7930-628-1, ISSN 1650-3163, Swedish Work Environment Authority (2015).
[16] F. Larsson, P. Andersson, P. Blomqvist, B.-E. Mellander, Toxic fluoride gas emissions from lithium-ion battery fires, Sci. Rep. 7 (2017) 10018.
[17] F. Larsson, P. Andersson, P. Blomqvist, A. Lorén, B.-E. Mellander, J. Power Sources 271 (2014) 414 420.
[18] F. Larsson, P. Andersson, P. Blomqvist, B.-E. Mellander, Gas emissions from Lithium-ion battery cells undergoing abuse from external fire, in: P. Andersson, B. Sundström (Eds.), Conference Proceedings of Fires in Vehicles (FIVE) 2016, Baltimore, 5-6 October 2016, SP Technical Research Institute of Sweden, Borås, Sweden, 2016, pp. 253 256.
[19] A. Lecocq, G.G. Eshetu, S. Grugeon, N. Martin, S. Laruelle, G. Marlair, J. Power Sources 316 (2016) 197 206.
[20] P. Ribière, S. Grugeon, M. Morcrette, S. Boyanov, S. Laruelle, G. Marlair, Energy Environ. Sci. 5 (2012) 5271 5280.
[21] P. Andersson, P. Blomqvist, A. Loren, F. Larsson, Fire Mater. 40 (2016) 999 1015.
[22] Y.-U. Park, D.-H. Seo, B. Kim, K.-P. Hong, H. Kim, S. Lee, R.A. Shakoor, K. Miyasaka, J.-M. Tarascon, K. Kang, Tailoring a fluorophosphate as a novel 4 V cathode for lithium-ion batteries, Sci. Rep. 2 (2012) 704.
[23] G.F. Ortiz, M.C. López, Y. Li, M.J. McDonald, M. Cabello, J.L. Tirado, Y. Yang, Enhancing the energy density of safer Li-ion batteries by combining high-voltage lithium cobalt fluorophosphate cathodes and nanostructured titania anodes, Sci. Rep. 6 (2016) 20656.
[24] A. Aboulaich, K. Ouzaouit, H. Faqir, A. Kaddami, I. Benzakour, I. Akalay, Mater. Res. Bull. 73 (2016) 362 368.
[25] Y.-K. Sun, M.-J. Lee, C.S. Yoon, J. Hassoun, K. Amine, B. Scrosati, Adv. Mater 24 (2012) 1192 1196.
[26] F. Larsson, B.-E. Mellander, J. Electrochem. Soc. 161 (10) (2014) A1611 A1617.
[27] P. Ping, Q. Wang, P. Huang, K. Li, J. Sun, D. Kong, C. Chen, J. Power Sources 285 (2015) 80 89.
[28] P. Huang, Q. Wang, K. Li, P. Ping, J. Sun, Sci. Rep. 5 (2015) 7788.
[29] Y. Fu, S. Lu, K. Li, C. Liu, X. Cheng, H. Zhang, J. Power Sources 273 (2015) 216 222.
[30] B. D. Gould, A. F. Durkin, H. V. Pham, F. W. Williams, Characterization of the heat release rate of lithium-ion battery failures from thermal abuse, 44th Power Sources Conference 2010, ISBN: 978-1-61782-064-9, Las Vegas, Nevada, USA, 14-17 June 2010, (2010) 5 7.
[31] T. Maloney, Extinguishment of lithium-ion and lithium-metal battery fires, U.S. Department of Transportation, 2014 DOT/FAA/TC-13/53, January 2014.
[32] X. Liu, Z. Wu, S.I. Stoliarov, Analysis of energy release during thermally-induced failure of lithium ion batteries: implications for vehicle fire safety, in: P. Andersson, B. Sundström (Eds.), Conference Proceedings of Fires in Vehicles (FIVE) 2016, Baltimore, 5-6 October 2016, SP Technical Research Institute of Sweden, Borås, Sweden, 2016, pp. 83 94.
[33] E.P. Roth, Abuse response of 18650 Li-ion cells with different cathodes using EC: EMC/$LiPF_6$ and EC: PC:DMC/$LiPF_6$ electrolytes, ECS Trans. 11 (19) (2008) 19 41 10.1149/1.2897969.
[34] C.-Y. Jhu, Y.-W. Wang, C.-M. Shu, J.-C. Chang, H.-C. Wu, Thermal explosion hazards on 18650 lithium ion batteries with a VSP2 adiabatic calorimeter, J. Hazard. Mater. 192 (2011) 99.
[35] Chia-Yuan Wen, Can-Yong Jhu, Yih-Wen Wang, Chung-Cheng Chiang, Chi-Min Shu, Thermal runaway features of 18650 lithium-ion batteries for $LiFePO_4$ cathode material by DSC and VSP2, J. Therm. Anal. Calorim. 109 (2012) 1297 1302.
[36] J. Vetter, P. Novák, M.R. Wagner, C. Veit, K.-C. Möller, J.O. Besenhard, M. Winter, M. Wohlfahrt-Mehrens, C. Vogler, A. Hammouched, J. Power Sources 147 (2005) 269 281.
[37] M. Klett, R. Eriksson, J. Groot, P. Svens, K. Ciosek Högström, R. Wreland Lindström, H. Berg, T. Gustafson, G. Lindbergh, K. Edström, J. Power Sources 257 (2014) 126 137.
[38] J. Groot, M. Swierczynski, A. Irina Stan, S. Knudsen Kær, J. Power Sources 286 (2015) 475 487.
[39] E.P. Roth, D.H. Doughty, J. Power Sources 128 (2004) 308 318.
[40] M.-S. Wu, P.-C.J. Chiang, J.-C. Lin, Y.-S. Jan, Electrochim. Acta 49 (2004) 1803 1812.
[41] P. Röder, B. Stiaszny, J.C. Ziegler, N. Baba, P. Lagaly, H.-D. Wiemhöfer, J. Power Sources 268 (2014) 315 325.
[42] Jianbo Zhang, Laisuo Su, Zhe Li, Ying Sun, Ningning Wu, Batteries 2 (2016) 12.
[43] M. Fleischhammer, T. Waldmann, G. Bisle, B.-I. Hogg, M. Wohlfahrt-Mehrens, J. Power Sources 274 (2015) 432 439.
[44] A. Friesen, F. Horsthemke, X. Mönnighoff, G. Brunklaus, R. Krafft, M. Börner, T. Risthaus, M. Winter, F.M. Schappacher, J. Power Sources 334 (2016) 1 11.
[45] J. Jeevarajan, Safety of commercial lithium-ion cells and batteries, in: Gianfranco Pistoia (Ed.), Lithium-ion Batteries Advances and Applications, Elsevier, Amsterdam, The Netherlands, 2014, pp. 387 407.
[46] R. Fathi, J.C. Burns, D.A. Stevens, H. Ye, C. Hu, G. Jain, E. Scott, C. Schmidt, J.R. Dahn, J. Electrochem. Soc. 161 (2014) A1572 A1579.
[47] S. Bertilsson, F. Larsson, M. Furlani, I. Albinsson, B.-E. Mellander, Lithium-ion battery electrolyte emissions analyzed by coupled thermogravimetric/Fourier-transform infrared spectroscopy, J. Power Sources 365 (2017) 446 455.
[48] S. Bertilsson, Thermal and Infrared Analysis of a Lithium-ion Battery Electrolyte and its Vapours for Safety Assessments, Master's Thesis Chalmers University of Technology, 2017.
[49] T. Osaka, D. Mukoyama, H. Nara, J. Electrochem. Soc. 162 (2015) A2529 A2537 and references therein.
[50] P. Singh, R. Vinjamuri, X. Wang, D. Reisner, Electrochim. Acta 51 (2006) 1673 1679.
[51] U. Westerhoff, K. Kurbach, F. Lienesch, M. Kurrat, Energy Technol. 4 (2016) 1620 1630.
[52] R.J. Harris, The Investigation and Control of Gas Explosions in Buildings and Heating Plants, British gas corporation, Midlands, England, 1983.
[53] F. Larsson, B.-E. Mellander, Energy storage system safety in electrified vehicles, in: P. Andersson, B. Sundström (Eds.), Conference proceedings of Fires in vehicles (FIVE) 2012, Chicago, 27-28 September 2012, SP Technical Research Institute of Sweden, Borås, Sweden, 2012, pp. 303 306.
[54] G. Eshetu, S. Grugeon, S. Laruelle, S. Boyanov, A. Lecocq, J.-P. Bertrand, G. Marlair, Phys. Chem. Chem. Phys. 15 (2013) 9145 9155.
[55] MSDS for EA, DMC and EC, https://www.sciencelab.com (accessed 13 July 2017).
[56] H. Yang, G.V. Zhang, P.N. Ross Jr., J. Power Sources 161 (2006) 573 579.
[57] H. Bohets, B.J. van der Veken, Phys. Chem. Chem. Phys. 1 (1999) 1817 1826.
[58] T.-K. Ha, C. Pal, P.N. Ghosh, Spectrochim. Acta 48A (8) (1992) 1083 1090.